Journal of the Korean Ceramic Society
Vol. 44, No. 7, pp. 343~348, 2007.

Fabrication and Characterization of Alumina/Silver Nanocomposites

Seung-Ho Cheon,* In-Sub Han,† and Sang-Kuk Woo

Energy Materials Research Center, Korea Institute of Energy Research, Daejeon 305-343, Korea
**The Research Institute of Daiyang Ind. Co., Icheon 467-813, Korea*
(Received June 28, 2007; Accepted July 23, 2007)

ABSTRACT

Alumina/silver nanocomposites were fabricated using a soaking method through a sol-gel route to construct an intra-type nanostructure. The pulse electric-current sintering (PECS) technique was used to sinter the nanocomposites. Several specimens were annealed after sintering. The microstructure, mechanical properties, critical frontal process zone (FPZ) size, and thermo-mechanical properties of the nanocomposites were estimated. The relative densities of the specimens sintered at 1350 and 1450°C were 95% and 99%, respectively. The maximum value of the three-point bending strength was found to be 780 MPa for the 2×2×10 mm specimen sintered at 1350°C. The fracture toughness of the specimen sintered at 1350°C was measured to be 3.60 MPa·$m^{1/2}$ using the single-edge V-notched beam (SEVNB) technique. The fracture mode of the nanocomposites was transgranular, in contrast to the intergranular mode of monolithic alumina. The fracture morphology suggested that dislocations were generated around the silver nanoparticles dispersed within the alumina matrix. The specimens sintered at 1350°C were annealed at 800°C for 5 min, following which the maximum fracture strength became 810 MPa and the fracture toughness improved to 4. 21 $MPam^{1/2}$. The critical FPZ size was the largest for the specimen annealed at 800°C for 5 min. Thermal conductivity of the alumina/silver nanocomposites sintered at 1350°C was 38 W/mK at room temperature, which was higher than the value obtained with the law of mixture.

Key words*: *Nanocomposite, Soaking method, Pulse Electric Current Sintering (PECS), Frontal Process Zone (FPZ) size, Single-edged V-Notch Beam (SEVNB)

1. Introduction

Alumina is widely regarded as a promising material for structural applications due to its desirable properties as a high-temperature material including its high refractoriness, hardness, good wear resistance, and chemical stability. However, its low fracture toughness and poor thermal shock resistance must be addressed before it can be utilized as an engineering material.[1)]

While the mechanical properties of structural ceramics are known to improve slightly by dispersing larger ceramic particles in ceramic-matrices,[2)] the nanocomposites proposed by Niihara et al. showed significantly improved mechanical properties.[3-7)] The nanocomposites were fabricated by dispersing nano-sized second phase particles within the matrix grains and along the grain boundaries. The thermal expansion mismatch between the matrix and second phase particles produces a marked improvement in a number of mechanical properties such as the fracture strength, fracture toughness, creep resistance, thermal shock resistance, and wear resistance. The mismatch of the thermal expansion around the nano-sized second phase particles induces shear stresses, which in turn generate dislocations. In addition, this process leads to the formation of sub-grain boundaries via the processes of dislocation rearrangement or reproduction; additionally, the expansion of the critical frontal process zone (FPZ) size ahead of a crack tip enhances the fracture toughness by creating nanocracks.[8)] This mechanism is fairly different from the particle-dispersed composites, where larger particles are dispersed within glassy materials generate cracks around the particles and improve the fracture toughness by a small amount.[2)]

It is known that the intra-type nanostructure generates dislocations and improves the mechanical properties of ceramics.[9,10)] However, the intra-type nanostructure is particularly difficult to fabricate using the conventional pressureless sintering technique or mixing processes. In this paper, alumina-based nanocomposites were fabricated using a soaking method through a sol-gel route to construct an intra-type nanostructure, in which a γ-alumina powder with high nanoporosity was used as the starting material.[10)]

The thermal expansion coefficients of the silver particles and alumina matrix are 22 and 8.8/MK,[11)] respectively. Dislocations will be easily generated along the alumina-silver boundaries as a result of the thermal expansion mismatch between the two materials.[12)] Alumina/silver nanocomposites will be particularly interesting as functional materials due to their excellent thermal conductivity as well as their

†Corresponding author : In-Sub Han
E-mail : ishan@kier.re.kr
Tel : +82-42-860-3147 Fax : +82-42-860-3133

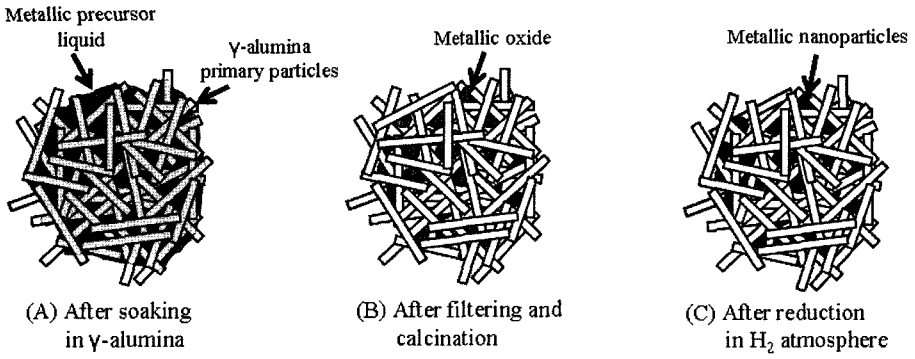

Fig. 1. Schematic description of the soaking method with γ-alumina powder and silver sulfate solution.

mechanical properties. The incorporation of nanoparticles with high thermal conductivity into a ceramic matrix may enhance the thermal conductivity of the ceramic-based nanocomposites and improve the thermal shock resistance. The microstructures of the sintered materials along with their mechanical properties (fracture strength, fracture toughness, and critical FPZ size) and thermo-mechanical properties are discussed here.

2. Experimental Procedure

2.1. Materials and procedure

Commercially available γ-alumina powder (AKP-G015, Sumitomo Chemical, Japan, purity 99.99%, 260 nm in average size) was used as the matrix of the nanocomposites,[10] and silver (I) sulfate (Ag_2SO_4, Osaka KISHIDA Chemistry, Japan, purity 99.5%) was used as nano-sized second phase particles dispersed within the matrix grains. 10 mass% α-alumina (AKP-53, Sumitomo Chemical, Japan, 99.99% purity, 0.3 μm average size) was used as a sintering seed. The γ-alumina powder and 1 M (mol/l) silver sulfate solution were prepared using a soaking method. The soaking method, schematized in Fig. 1, can be explained as follows. First, the γ-alumina powder was soaked in the silver sulfate solution in a vacuum. Second, the γ-alumina/silver sulfate solution composite powder was centrifuged for 30 min at 3000 rpm to remove the excess silver sulfate solution from the surface of the agglomerated γ-alumina powder and was then filtered to fabricate an intra-type nanostructured powder. Third, the mixed powder was calcined at 550°C for 3 h in air to obtain silver oxide particles in the pores of the γ-alumina powder. Finally, the calcined powder was reduced in hydrogen atmosphere for 2 h at 800°C to obtain metallic silver nanoparticles.

The specimens were sintered using the pulse electric-current sintering (PECS) technique at 1250, 1350, and 1450°C for 5 min under 30 MPa in a vacuum. The volume fraction of the silver particles was approximately 1 vol%. The specimens sintered at 1350°C were then annealed for 5 min at 700, 750, 800, 850, and 900°C in an argon atmosphere.

2.2. Characterization

The relative density of the sintered specimens was measured using the Archimedes method. The crystal phases of the calcined powder, reduced powder, and sintered specimens were analyzed by X-ray diffraction (SHIMADZU, XD-D1, Japan). The fracture strength was measured using a three-point bending test on 2×2×10 mm specimens with an 8-mm span and a cross-head speed of 0.5 mm/min. The fracture toughness was measured using the single-edge V-notched beam (SEVNB) method.[13] After the three-point bending test, the fracture surfaces were observed via a scanning electron microscopy (SEM) (JEOL, JSM-6360LV, Japan).

The thermal diffusivity and heat capacity of the nanocomposites were measured by means of the laser-flash method (Ulvac Shinku-Riko, Flash Constant Analyzer, TC-7000, Japan). The thermal conductivity of the nanocomposites was calculated by multiplying the thermal diffusivity, heat capacity and bulk density. The specimens were prepared in the form of circular disks 10 mm in diameter and 1 mm in thickness.

3. Results and Discussion

Fig. 2 shows a TEM micrograph of the agglomerated γ-alumina powder with silver nanoparticles prepared via the

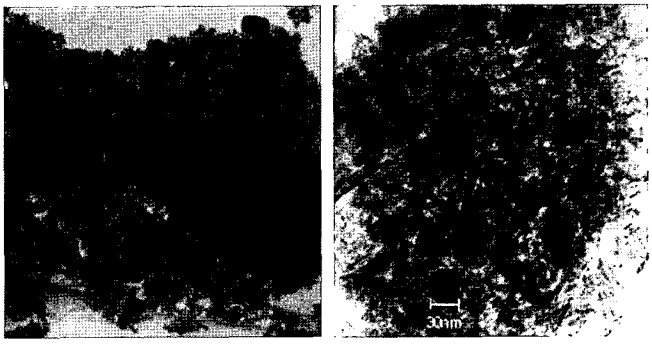

Fig. 2. TEM micrograph of reduced silver particles within γ-alumina agglomerates.

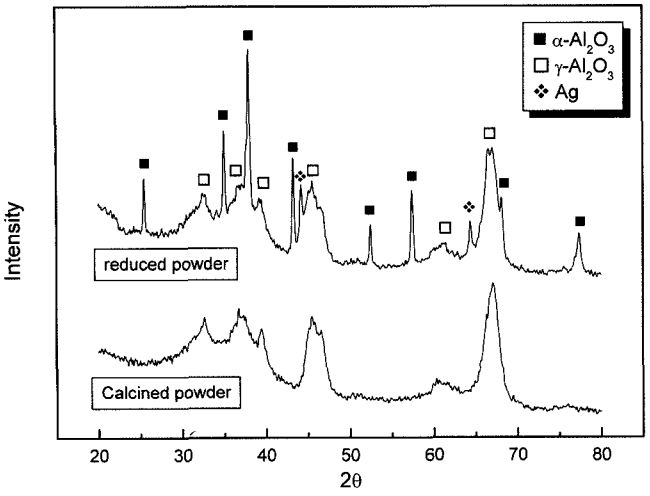

Fig. 3. XRD patterns of calcined and reduced powders for alumina/silver nanocomposites.

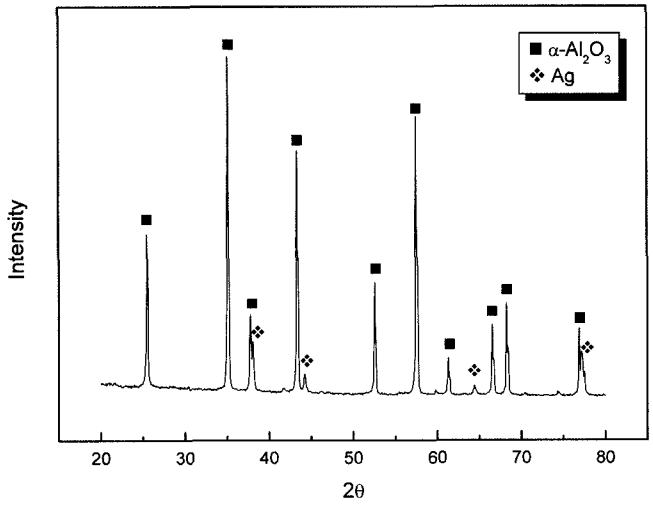

Fig. 4. XRD patterns of sintered specimen for alumina/silver nanocomposites.

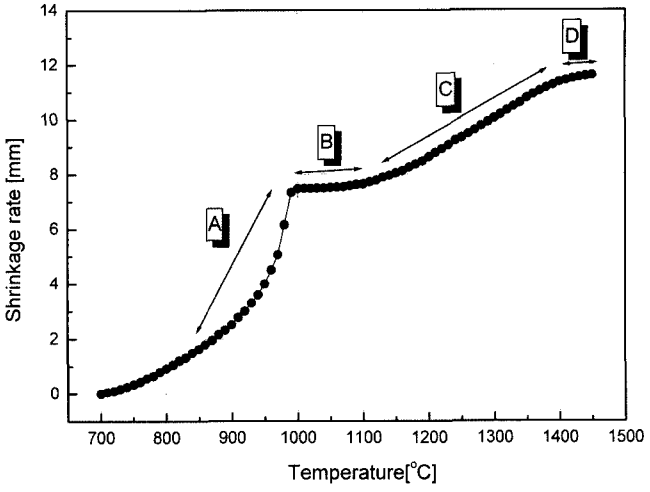

Fig. 5. The shrinkage rate of alumina/silver nanocomposites during pulse electric current sintering.

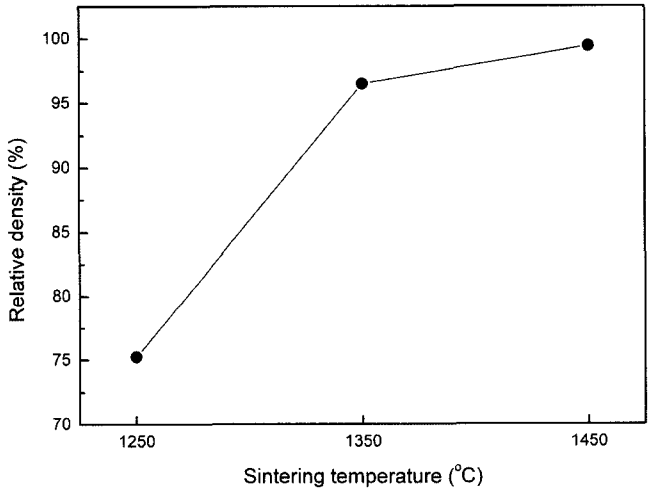

Fig. 6. Relative densities of the sintered specimens as a function of sintering temperatures.

soaking method after reducing in a hydrogen atmosphere. Silver nanoparticles are observed within the agglomerated γ-alumina powder. It can be observed that metallic silver particles with an average grain size of 30 nm are dispersed within the γ-alumina agglomerates: primary particles of the γ-alumina with a needle-like shape are observed as well.

XRD patterns of the calcined and reduced powders and the sintered specimen for the alumina/silver nanocomposites are shown in Figs. 3 and 4, respectively. In Fig. 3, most of the XRD peaks of the calcined powder are due to the glassy phase of γ-alumina. In addition, metallic silver and α-alumina can be observed in the reduced powder. Fig. 4 shows the XRD patterns of the specimen sintered at 1350°C, in which α-alumina is the main phase coexisting with the metallic silver phase.

Fig. 5 shows the shrinkage rate as a function of the temperature to monitor the phase transition of alumina nanocomposite specimens during sintering by the PECS technique. The [A] range in Fig. 5 represents the phase transition of alumina with a large specific volume reduction. γ-alumina transforms into δ-alumina at 850°C and then into θ-alumina at 900°C. A further increase of 100°C in the sintering temperature results in a transformation into α-alumina with maximum densification during sintering. In addition, the relative densities change from 3.6 - 3.65 g/cm^3 in the θ-alumina phase (a spinel structure with cubic close packing of the oxygen sublattice) to 3.98 g/cm^3 in the α-alumina phase (a corundum structure with hexagonal close packing of the oxygen sublattice).[14] As illustrated in Fig. 5, the [B] range of 1000 - 1100°C appears to correspond to a rearrangement, which is likely to be in a liquid sintering procedure. The [C] and [D] ranges represent the densification and grain growth as well as the stabilization stages, respectively.

The relative densities of the specimens sintered at several different temperatures are shown in Fig. 6. The specimen

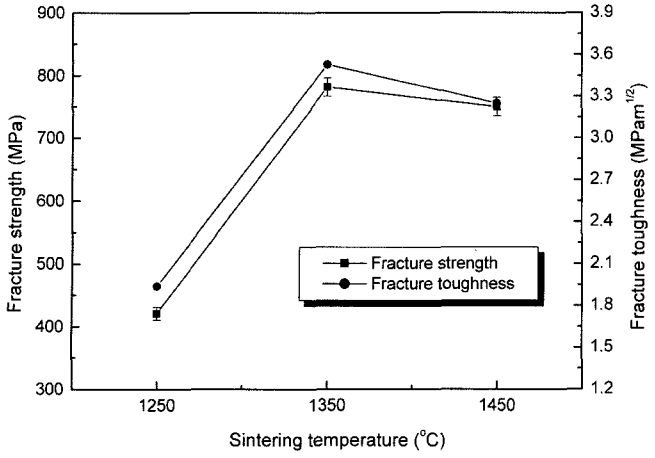

Fig. 7. Strength and fracture toughness of the sintered specimens as a function of sintering temperatures.

not fully densified at 1250°C shows 75% relative density. However, the densities of alumina/silver nanocomposites are enhanced as the sintering temperature increases: the specimens sintered at 1350°C and 1450°C showed 95% and 99% relative densities, respectively.

The mechanical properties, in this case the three-point bending strength and fracture toughness, are shown in Fig. 7. The maximum strength of the alumina/silver nanocomposite was 780 MPa for a specimen sintered at 1350°C, while the maximum fracture toughness for a specimen sintered at 1350°C was 3.60 $MPam^{1/2}$. The strength and fracture toughness of the specimen sintered at 1450°C was slightly lower due to coarsening of the matrix grains at the higher sintering temperature. Moreover, dislocations generated around the silver nanoparticles in the alumina matrix will migrate outside the matrix grains at higher temperatures. Compared with the values for monolithic alumina (520 MPa and 3.78 $MPam^{1/2}$) measured previously,[10] the

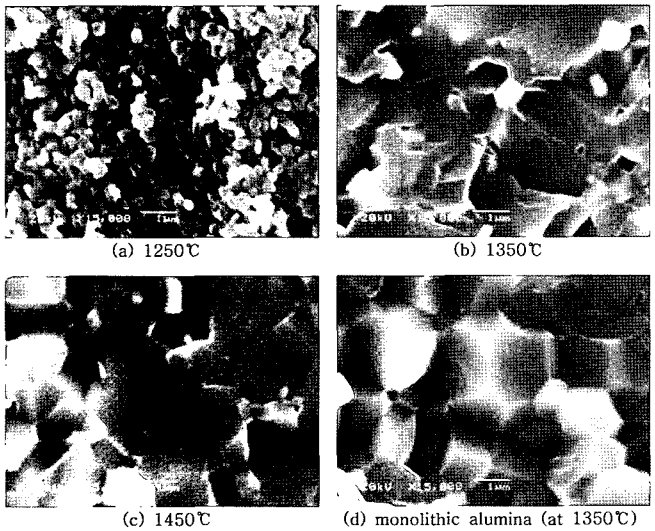

Fig. 8. SEM micrographs of the fracture surfaces of alumina/silver nanocomposites and monolithic alumina at various sintering temperature.

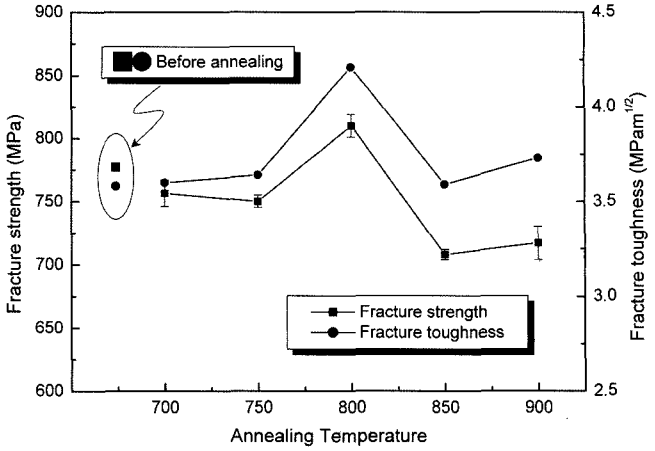

Fig. 9. Strength and fracture toughness vs. annealing temperatures for the specimens sintered at 1350°C and annealed for 5 min.

nanocomposites sintered at 1350°C and 1450°C show a higher fracture strength with a slight reduction in the fracture toughness.

Fig. 8 shows SEM micrographs of the fracture surfaces of nanocomposites sintered at (a) 1250°C (b) 1350°C, (c) 1450°C; (d) shows monolithic alumina sintered at 1350°C. The fracture mode of nanocomposites with dislocations around the second-phase silver nanoparticles within the alumina matrix was found to be transgranular, in contrast to the intergranular fracture mode of the monolithic alumina (d). Thus, the nanocomposites show an improvement of strength due to the decrease in residual stresses in the alumina matrix and along the grain boundaries. Davidge et al. also reported dramatic differences in the abrasive wear surfaces between monolithic alumina and nanocomposites: in their study, the surface of monolithic alumina showed grain pullout, while the nanocomposites showed a ground or abraded surface due to the improved strength along the grain boundaries.[15]

Fig. 9 shows the strength and fracture toughness versus the annealing temperature for the specimens sintered at 1350°C and annealed for 5 min. The maximum strength and fracture toughness of the specimen annealed at 800°C were 810 MPa and 4.21 $MPam^{1/2}$, respectively. It is also known that the annealing temperatures below 800°C have only a slight effect on the strength and fracture toughness, which implies that dislocations become active only at higher temperatures above 750°C.

The fracture toughness of ceramics can be improved by expanding the critical FPZ size ahead of the crack tip,[16] as ceramics with larger critical FPZ size consume relatively more fracture energy during crack extensions and consequently have a higher fracture toughness. In this section, the relationship between the experimentally obtained strength and fracture toughness and the calculated critical FPZ size is discussed for the as-sintered and annealed nanocomposites. As a theoretical explanation of this relationship is reported elsewhere,[16] it is only briefly described here.

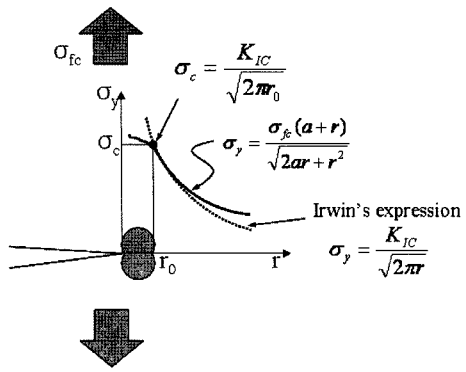

Fig. 10. Critical stress state ahead of a crack tip in an infinite plate with a long crack.

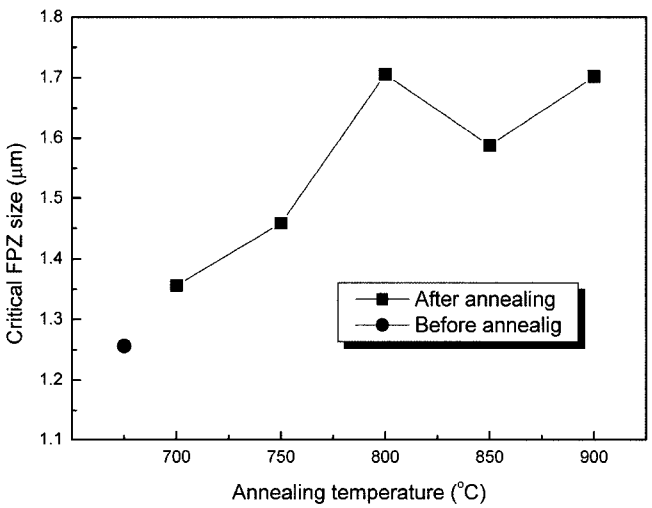

Fig. 11. Relation between the critical frontal process zone sizes and annealing temperatures for the specimens sintered at 1350°C.

Fig. 10 shows the critical stress state ahead of a crack tip in an infinite plate, in which the critical FPZ size is defined as r_0 on the r-axis and the critical local stress, σ_c, corresponds to the stress at r_0. A case in which the crack is sufficiently long enough compared with the critical FPZ size is considered, and Irwin's K_I value approximation is applicable at r_0. Thus, the following relationship is derived at r_0 under the critical state:

$$\sigma_C = \frac{K_{IC}}{\sqrt{2\pi r_0}} \tag{1}$$

Here, K_{IC} is the fracture toughness. The critical FPZ size can be calculated using the relationship between the bending strength, σ_B, and the critical local stress, σ_c, using Weibull statistics[16]:

$$\frac{\sigma_C}{\sigma_B} = \left\{\frac{V_B}{V_{FPZ}}\right\}^{1/m} \tag{2}$$

In Eq. 2, m represents the shape parameter of the Weibull distribution and V_B and V_{FPZ} are the effective volumes of the flexure specimen and critical FPZ, respectively. V_B and V_{FPZ} can be expressed as[16]

$$V_B = \frac{V}{2(m+1)^2} \tag{3}$$

and

$$V_{FPZ} = 3.29 r_0^2 B \tag{4}$$

V represents the volume of the flexure specimen (V=B (thickness)×H (height)×S (span)).

First, an assumed r_0 value must be utilized. V_{FPZ} is then calculated from Eq. (4). Second, σ_c is estimated using Eqs. (3) and (2). Finally, r_0 is obtained from Eq. (1). If the calculated r_0 value differ from the assumed value, the calculation process must then be reported using a newly assumed r_0 value.

Fig. 11 shows the calculated critical FPZ size of the as-sintered and annealed nanocomposites under the assumption that m is 20 in Eqs. (2) and (3). It was found that the annealed nanocomposites have a larger critical FPZ size compared with the as-sintered nanocomposites and that the critical FPZ size of the nanocomposites annealed at 800°C has the largest value. Although the fracture toughness levels of the specimens annealed at 850°C and 900°C show lower values compared to those of the as-sintered nanocomposites, the critical FPZ sizes of the specimens annealed at 850°C and 900°C are nonetheless large. Thus, it is conceivable that in the matrix grain, there will be migration of dislocations if a proper annealing temperature is used and the nano-crack formation around the dislocations will expand the critical FPZ size on the basis of a toughening mechanism that was proposed previously.[8]

The thermal conductivity of the alumina/silver nanocomposite at room temperature was 38 W/mK for the specimen sintered at 1350°C, which was higher than the value calculated with the law of mixture, as shown in Fig. 12. The thermal conductivity of the monolithic alumina (30 W/mK) will be improved slightly due to the dispersion of silver nanopar-

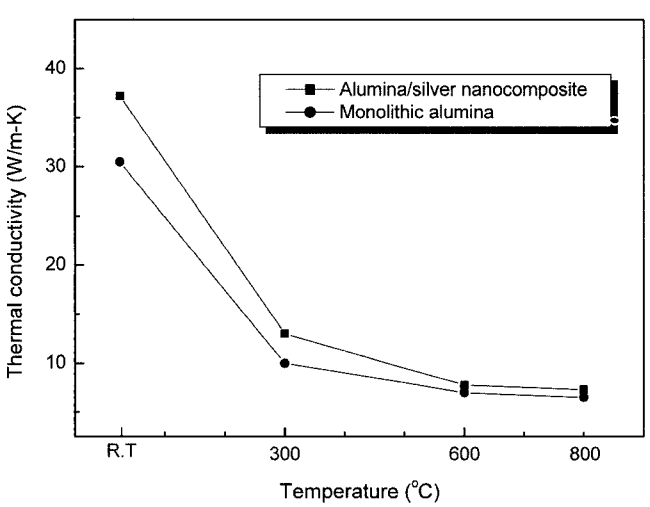

Fig. 12. Thermal conductivities of the alumina/silver nanocomposites and monolithic alumina sintered at 1350°C.

ticles. However, the high thermal conductivity of the nanocomposites mainly results from the release of sintering residual stresses in the alumina matrix by the formation of dislocations, which activates the phonon as a carrier of heat.

4. Conclusions

Alumina/silver nanocomposites were fabricated using a soaking method through the sol-gel route in combination with pulse electric-current sintering (PECS) to yield an alumina-based intra-type nanostructure. The maximum fracture strength of the as-sintered alumina/silver nanocomposites was 780 MPa for a specimen sintered at 1350°C: the maximum fracture toughness was 3.60 $MPam^{1/2}$ obtained via the single-edge V-notched beam (SEVNB) technique for a specimen sintered at 1350°C. The fracture mode of the as-sintered nanocomposites with dislocations around the silver nanoparticles within the alumina matrix is transgranular in contrast to the intergranular fracture mode of monolithic alumina. The maximum fracture strength of the annealed nanocomposites for the specimen annealed at 800°C was 810 MPa, and the fracture toughness was 4. 21 $MPam^{1/2}$. The marked improvement in the fracture toughness can be explained by the expansion of the critical frontal process zone (FPZ) size. Thermal conductivity of the alumina/silver nanocomposite was 38 W/mK at room temperature for the specimen sintered at 1350°C, which was higher than the value obtained with the law of mixture. Thus, alumina/silver nanocomposites are interesting as functional materials due to their high thermal conductivity as well as their mechanical properties.

REFERENCES

1. D. O'Sullivan, M. Poorteman, P. Descamps, F. Cambier, A. Leriche, and B. Thierry, "Optimization of Alumina-Silicon Carbide Dispersion and the Fabrication of Nanocomposites Ceramic Materials," *Key Eng. Mater.*, **9-100** 247-56 (1995).
2. R. W. Davidge and T. J. Green, "The Strength of Two-phase Ceramic/glass Materials," *J. Mater. Sci.*, **3** 629-34 (1968).
3. K. Niihara, "New Design Concept of Structural Ceramics-ceramic nanocomposites," *J. Ceram. Soc. Jpn.*, **99** 974-81 (1991).
4. K. Niihara and A. Nakahira, "Particulate Strengthened Oxide Ceramics-Nanocomposites"; pp. 637-44, Advanced Structural Inorganic Composites, P. Vincenzini (Editor), Elsevier Science Publishers B. V., 1991.
5. M. Nawa, T. Sekino, and K. Niihara, "Microstructure and Mechanical Properties of Al_2O_3/Mo Nanocomposites," *Japan Society of Powder and Powder Metallurgy*, **39** [12] 1104-8 (1992).
6. T. Ohji, Y. K. Jeong, Y. H. Choa, and K. Niihara, "Strengthening and Toughening Mechanisms of Ceramic Nanocomposites," *J. Am. Ceram. Soc.*, **81** [6] 1453-60 (1998).
7. H. kondo, T. sekino, Y. H. Choa, and K. Niihara, "Mechanical Properties of 3Y-ZrO_2/Ni Composites Prepared by Reductive Sintering," *Key Eng. Mater.*, **161-163** 419-22 (1999).
8. H. Awaji, S. M. Choi, and E. Yagi, "Mechanisms of Toughening and Strengthening in the Ceramic-based Nanocomposites," *Mechanics of Materials*, **34** 411-22 (2002).
9. S. M Choi and H. Awaji, "Nanocomposites-A New Material Design Concept," *Sci. and Tech. of Advanced Mater.*, **6** 2-10 (2005).
10. U. Leela-adisorn, T. Matsunaga, Y. Kobayashi, S. M. Choi, and H. Awaji, "Soaking Method for Fabrication of Alumina-based Nanocomposites," *Ceramics Int.*, **31** 803-09 (2005).
11. W. B. Chou and W. H. Tuan, "Toughening and Strengthening of Alumina with Silver Inclusions," *J. Euro. Ceram. Soc.*, **15** 291-95 (1995).
12. H. Awaji, S-M. Choi, and E. Yagi, "Mechanisms of Toughening and Strengthening in Ceramic-based Nanocomposites," *Mech. of Mater.*, **34** 411-22 (2002).
13. H. Awaji and Y. Sakaida, "V-Notch Technique for Single-edge Notched Beam and Chevron Notch Methods," *J. Am. Ceram. Soc.*, **73** [11] 3522-23 (1990).
14. I. Levin and D. Brandon, "Metastable Alumina Polymorphs: Crystal. Structures and Transition Sequences," *J. Am. Ceram. Soc.*, **81** [8] 1995-2012 (1998).
15. R. W. Davidge, R. J. Brook, F. Cambier, M. Poorteman, A. Leriche, D. O'Sullivan, S. Hampshire, and T. Kennedy, "Fabrication, Properties, and Modelling of Engineering Ceramics Reinforced with Nanoparticles of Silicon Carbide," *British Ceramic Transaction*, **96** [3] 121-27 (1997).
16. H. Awaji., T. Matsunaga, and S. M. Choi, "Relation between Strength, Fracture Toughness, and Critical Frontal Process Zone Size in Ceramic," *Materials Trans.*, **47** 1532-39 (2006).